



HAL
open science

Precise Modulation of Carbon Activity Sites in Metal-Free Covalent Organic Frameworks for Enhanced Oxygen Reduction Electrocatalysis

Jianchuan Liu, Jie Zhao, Cuiyan Li, Yaozu Liu, Daohao Li, Hui Li, Valentin Valtchev, Shilun Qiu, Yujie Wang, Qianrong Fang

► **To cite this version:**

Jianchuan Liu, Jie Zhao, Cuiyan Li, Yaozu Liu, Daohao Li, et al.. Precise Modulation of Carbon Activity Sites in Metal-Free Covalent Organic Frameworks for Enhanced Oxygen Reduction Electrocatalysis. *Small*, 2023, pp.2305759. 10.1002/sml.202305759 . hal-04280297

HAL Id: hal-04280297

<https://hal.science/hal-04280297>

Submitted on 10 Nov 2023

HAL is a multi-disciplinary open access archive for the deposit and dissemination of scientific research documents, whether they are published or not. The documents may come from teaching and research institutions in France or abroad, or from public or private research centers.

L'archive ouverte pluridisciplinaire **HAL**, est destinée au dépôt et à la diffusion de documents scientifiques de niveau recherche, publiés ou non, émanant des établissements d'enseignement et de recherche français ou étrangers, des laboratoires publics ou privés.

Precise Modulation of Carbon Activity Sites in Metal-Free Covalent Organic Frameworks for Enhanced Oxygen Reduction Electrocatalysis

Jianchuan Liu,[‡] Jie Zhao,[‡] Cuiyan Li, Yaozu Liu, Daohao Li, Hui Li, Valentin Valtchev, Shilun Qiu, Yujie Wang* and Qianrong Fang**

J. Liu, Dr. C. Li, Dr. Y. Liu, Dr. H. Li, Dr. Y. Wang, Prof. S. Qiu, Prof. Q. Fang,

State Key Laboratory of Inorganic Synthesis and Preparative Chemistry, Jilin University, Changchun 130012, P. R. China.

E-mail: qrfang@jlu.edu.cn or wyujie@jlu.edu.cn

Dr. J. Zhao

SINOPEC Research Institute of Petroleum Processing, P. R. China

Prof. D. Li

State Key Laboratory of Bio-fibers and Eco-textiles, College of Materials Science and Engineering, Qingdao University, Qingdao 266071, P. R. China

E-mail: lidaohao@qdu.edu.cn

Prof. V. Valtchev

Qingdao Institute of Bioenergy and Bioprocess Technology, Chinese Academy of Sciences, 189 Songling Road, Laoshan District, Qingdao, Shandong 266101, P. R. China; Normandie Univ, ENSICAEN, UNICAEN, CNRS, Laboratoire Catalyse et Spectrochimie, 6 Marechal Juin, 14050 Caen, France

[‡] These authors contributed equally.

Abstract:

Metal-free carbon-based materials have gained recognition as potential electrocatalysts for the oxygen reduction reaction (ORR) in new environmentally-friendly electrochemical energy conversion technologies. The presence of effective active centers is crucial for achieving productive ORR. In this study, we present the synthesis of two metal-free dibenzo[a,c]phenazine-based covalent organic frameworks (DBP-COFs), specifically JUC-650 and JUC-651, which serve as ORR electrocatalysts. Among them, JUC-650 demonstrates exceptional catalytic performance for ORR in alkaline electrolytes, exhibiting an onset potential of 0.90 V vs RHE and a half-wave potential of 0.72 V vs RHE. Consequently, JUC-650 stands out as one of the most outstanding metal-free COF-based ORR electrocatalysts reported to date. Experimental investigations and density functional theory calculations confirm that modulation of the frameworks' electronic configuration allows for the reduction of adsorption energy at the Schiff-base carbon active sites, leading to more efficient ORR processes. Moreover, the DBP-COFs can be assembled as excellent air cathode catalysts for zinc-air batteries (ZAB), rivaling the performance of commercial Pt/C. This study provides valuable insights for the development of efficient metal-free organoelectrocatalysts through precise regulation of active site strategies.

Keywords: covalent organic framework, oxygen reduction reaction, metal-free electrocatalyst, porous materials, Zn-air battery

1. Introduction

The development of metal-free carbon-based electrocatalysts for the oxygen reduction reaction (ORR) is of paramount importance in advancing the widespread applications of emerging energy storage and conversion systems.^[1-4] One promising approach to enhancing the catalytic activity, selectivity, and stability of electrocatalysts is the establishment and modulation of active sites.^[5,6] These active sites possess favorable electronic and geometric properties that facilitate the adsorption and activation of oxygen molecules, effectively driving the ORR process.^[7-9] Over the past few decades, an extensive body of literature has reported numerous metal-free carbon-based catalysts with features including heteroatom doping, defect effects, edge exposure, and composite structures.^[10-21] However, the complex and demanding synthesis processes associated with these materials present challenges concerning the density and uncertainty of active sites.^[22-24] The resulting ambiguity in catalytic systems due to these uncontrollable factors has become a major obstacle in the development of efficient metal-free carbon-based electrocatalysts. A profound understanding of the relationship between active sites and catalytic mechanisms is therefore crucial in further improving the performance of ORR electrocatalysts.^[25-27] Consequently, the exploration and manipulation of active sites in ORR electrocatalysts offer a promising pathway for surmounting the limitations of traditional catalysts and advancing the development of efficient energy conversion technologies.

Covalent organic frameworks (COFs) have emerged as a class of organic porous materials, garnering substantial attention across various research fields due to their

structural regularity, high crystallinity, and significant porosity.^[28-38] Notably, their exceptional designability at the molecular level positions COFs as highly promising materials in the development and application of sustainable energy technologies, including electrocatalysis, photocatalysis, and energy storage.^[39-51] Previous studies have indicated that by precisely controlling the electronic distribution of ORR electrocatalysts, the adsorption capacity for oxygen intermediates can be optimized, thus reducing reaction barriers.^[52] Consequently, the judicious incorporation of specific functional groups/heterocycles as building units into conjugated frameworks represents an effective and practical strategy for enhancing the intrinsic catalytic activity of electrocatalysts.^[53-55] For instance, the introduction of structural units such as thiophene, bithiophene, benzo-[c][1,2,5]trithiophene, thiophene[3,2-b]thiophene, and benzotrithiophene, alongside other aromatic fused heterocyclic compounds, has been reported to exhibit excellent electrocatalytic properties.^[56-60] Furthermore, these studies have elucidated the underlying mechanisms governing ORR activity, thereby providing valuable reference and guidance for the development of efficient catalysts. Therefore, achieving precise structural design and clear modulation of active sites is not only necessary but also poses a significant challenge in the pursuit of efficient electrocatalysts.

In this study, we employed benzo[a,c]phenazine as a central structure for constructing nitrogen-doped planar 4-connected aldehyde ligands, which were coupled with two different conjugated 4-connected amine linkers. This approach successfully synthesized two novel benzo[a,c]phenazine-based covalent organic

frameworks (COFs), namely DBP-COFs (JUC-650 and JUC-651, JUC = Jilin University China). Among them, JUC-650 exhibited a high onset potential of 0.90 V vs RHE and an excellent half-wave potential of 0.72 V vs RHE. Furthermore, the JUC-650-based Zn-air battery (ZAB) demonstrated a high specific capacity of 722.6 mAh g_{Zn}⁻¹, comparable to that of commercial Pt/C. Additionally, we optimized the synthesis procedure and successfully synthesized TFPPy-PyTTA-COF to compare the differences in intrinsic activity.^[61] The uneven distribution of π conjugation structures may lead to uneven local charge distribution, resulting in the formation of charge-polarized regions. This phenomenon facilitates the adsorption and activation of oxygen molecules during ORR. Density functional theory (DFT) calculations supported the experimental results. The enriched electron density of JUC-650 excited the Schiff-base carbons with higher positive potential, serving as active centers and reducing the adsorption energy barrier for oxygen intermediates in the rate-determining step of ORR. These findings confirm that precise modulation of the overall electronic characteristics of the COF framework can effectively control the ORR activity of metal-free COFs at the Schiff base carbon sites.

2. Results and Discussion

2.1 Experiment and Structural Determination of DBP-COFs

The classical Schiff base reaction was employed as the synthesis strategy. As depicted in **Scheme 1**, the quadrilateral building blocks, 3,6,11,12-tetrakis(4-aldehydephenyl) dibenzo[a,c]phenazine (TADDP) as an aldehyde ligand and 4,4',4'',4'''-(1,3,6,8-Pyrenetetrayl) tetrakis [benzenamine] (PyTTA) and

N1,N1,N4,N4-Tetrakis(4-aminophenyl)-1,4-benzenediamine (TAPDA) as amino ligands, were individually placed in a dioxane/mesitylene solution system. The reaction was then carried out by solvothermal method at 120 °C for 72 h. Following the reaction, the resulting solids were washed with acetone and soaked in N, N-dimethylformamide (DMF) for 12 h to eliminate residual solvents and unreacted precursors. Subsequently, DMF was removed through Soxhlet extraction using acetone for three days at 80 °C. After vacuum drying an orange-red (JUC-650) and a reddish-brown (JUC-651) solid was obtained, with yields of 85% and 81%, respectively. To facilitate subsequent electrochemical tests, the TFPPy-PyTTA-COF was also synthesized via the optimized synthesis approach, yielding a yellow solid, serving as a reference sample (Scheme S3).

The cell parameters and crystallinity of the newly synthesized COF materials were confirmed through powder X-ray diffraction (PXRD) experiments, followed by simulation and refinement using Materials Studio software (Figure 1).^[62] The structural simulation revealed that JUC-650 and JUC-651 exhibited irregular channels based on the structural characteristics of TADDP. To compare different stacking modes, a geometric energy minimization method was employed. The experimental data corresponded to the diffraction peaks of the AA stacking mode (Figures S1 and S2). The cell parameters of the repeated TFPPy-PyTTA-COF were consistent with the literature values (Figure S3). Full profile pattern matching (Pawley) refinements were conducted using the PXRD patterns. The peaks were observed for JUC-650 at $2\theta = 4.96, 5.77, 8.12, 9.92, 11.31$ and 14.03° corresponded to the (110), (200), (020), (220),

(400), and (420) planes, respectively (Figure 1a). Similarly, for JUC-651, the peaks at $2\theta = 4.32, 5.21, 5.75, 8.63, 9.09, 10.46, 11.54$ and 12.99° corresponded to the (010), (110), (200), (300), (120), (220), (400) and (030) planes, respectively (Figure 1b). The unit cell parameters were determined as follows: $a = 31.2949 \text{ \AA}$, $b = 22.8199 \text{ \AA}$, $c = 3.8806 \text{ \AA}$, $\alpha = 101.1008^\circ$, $\beta = 87.3264^\circ$, $\gamma = 91.3280^\circ$ for JUC-650; $a = 30.7174 \text{ \AA}$, $b = 20.6486 \text{ \AA}$, $c = 3.9596 \text{ \AA}$, $\alpha = 81.4733^\circ$, $\beta = 91.8105^\circ$, $\gamma = 90.7443^\circ$ for JUC-651; and $a = 24.99617 \text{ \AA}$, $b = 25.39614 \text{ \AA}$, $c = 7.22340 \text{ \AA}$, $\alpha = 107.01436^\circ$, $\beta = 91.63419^\circ$, $\gamma = 90.20908^\circ$ for TFPPy-PyTTA-COF, respectively (Tables S2 and S3). The theoretically simulated values based on the refined cell parameters closely matched the experimental results (JUC-650: $a = 30.7187 \text{ \AA}$, $b = 22.8989 \text{ \AA}$, $c = 3.9687 \text{ \AA}$, $\alpha = 107.7469^\circ$, $\beta = 88.0172^\circ$, $\gamma = 91.7587^\circ$, $R_p = 2.76\%$, $R_{wp} = 4.14\%$; JUC-651: $a = 30.6634 \text{ \AA}$, $b = 20.4884 \text{ \AA}$, $c = 3.9331 \text{ \AA}$, $\alpha = 81.6733^\circ$, $\beta = 91.9959^\circ$, $\gamma = 91.5037^\circ$, $R_p = 2.14\%$, $R_{wp} = 2.81\%$; and TFPPy-PyTTA-COF: $a = 24.99941 \text{ \AA}$, $b = 25.39129 \text{ \AA}$, $c = 7.22353 \text{ \AA}$, $\alpha = 107.02472^\circ$, $\beta = 91.64241^\circ$, $\gamma = 90.21138^\circ$, $R_p = 1.65\%$, $R_{wp} = 2.14\%$).

2.2 Characterization of DBP-COFs

To determine the specific surface areas and porosity of JUC-650 and JUC-651 materials, nitrogen adsorption and desorption isotherms were measured at 77 K. The adsorption isotherms of JUC-650 and JUC-651 exhibited a type-I isotherm, providing strong evidence for the microporous structure of the materials (Figure 1c and 1d). The Brunauer-Emmett-Teller (BET) surface areas of JUC-650 and JUC-651 were determined to be $694.52 \text{ m}^2 \text{ g}^{-1}$ and $596.72 \text{ m}^2 \text{ g}^{-1}$, respectively. Pore-size distribution

analysis, conducted through nonlocal density functional theory (NLDFT), demonstrated that JUC-650 exhibited a microporous structure with a pore size of 1.00 nm, while JUC-651 also displayed a microporous nature with a slightly larger pore size of 1.18 nm (Figure 1c and 1d. Insert: pore-size distributions; Figures S4-S9).

The synthesis of JUC-650 and JUC-651 from a bonding perspective was studied using Fourier transform infrared (FT-IR) spectroscopy. As shown in Figure 2a and 2b, the disappearance of peaks at 1701 cm^{-1} (C=O band for TADDP) and $3464\sim 3344\text{ cm}^{-1}$ (N-H band for PyTTA and TAPDA), along with the appearance of characteristic peaks located at 1625 cm^{-1} (C=N band for JUC-650 and JUC-651), fully demonstrated the interaction between the amine and aldehyde groups (Figures S10 and S11). The solid-state ^{13}C cross-polarization magic-angle-spinning nuclear magnetic resonance (^{13}C CP/MAS NMR) spectra further confirmed the successful synthesis of the materials. The typical C=N signals were detected at chemical shifts of approximately 157.6 ppm for both COFs (Figure 2c and 2d). Other bond chemical shift signals are shown in Figures S12 and S13. To further confirm the composition of the COFs, ex-situ X-ray photoelectron spectroscopy (XPS) was conducted. The XPS spectra illustrates the initial C 1s and initial N 1s spectra of the COFs electrode (Figures S14 a and b). The C 1s spectra can be resolved into four peaks corresponding to C=C (284.2 eV), C-C (284.8 eV), C-N (285.5 eV), and C=N (287.2 eV). Meanwhile, the initial N 1s spectra can be decomposed into two peaks attributed to C-N (399.5 eV) and C=N (400.5 eV).

Noteworthy, JUC-650 and JUC-651 exhibited outstanding thermal and chemical stability. The thermogravimetric (TGA) analysis curves revealed that JUC-650 retained its original crystal structure up to 450 °C, while JUC-651 exhibited noticeable weight loss at 430 °C (Figures S15 and S16). Interestingly, both COFs maintained the crystallinity of their frameworks even after one year in ambient air. The chemical stability of JUC-650 and JUC-651 was further explored by subjecting them to harsh chemical environments, including 3M HCl, 3M NaOH solutions, and various organic solvents (dimethylformamide, dichloromethane, tetrahydrofuran, acetone, ethanol, and n-hexane) for 24 h. The stable framework structures of JUC-650 and JUC-651 remained intact (Figures S17 and S18). These results demonstrate the excellent chemical stability of JUC-650 and JUC-651, laying a solid foundation for their development and application as oxygen reduction catalysts.

The morphology of JUC-650 and JUC-651 was further examined using scanning electron microscopy (SEM) and transmission electron microscopy (TEM). The SEM images revealed the curved sheet-shaped morphology of JUC-650 and the irregular particle morphology of JUC-651 (Figures S19 and S20). Additionally, the TEM images displayed the interlayer texture of both structures, unveiling their two-dimensional (2D) network properties (Figures 2e, 2f, S21 and S22). Energy-dispersive X-ray spectroscopy (EDS) spectra further confirmed the homogeneous distribution of C and N atoms in DBP-COFs (Figures 2g, 2h, S23 and S24).

2.3 ORR Catalytic Activity

To evaluate the electrocatalytic oxygen reduction activity of DBP-COFs, linear sweep voltammetry (LSV) tests were conducted in a 0.1 M KOH aqueous solution saturated with oxygen and scan rates ranging from 400 to 2500 rpm. As a reference sample, TFPPy-PyTTA-COF was employed. JUC-650 exhibited superior catalytic activity than others at 1600 rpm, with an onset potential (E_{onset}) of 0.90 V *vs* RHE, a half-wave potential ($E_{1/2}$) of 0.72 V *vs* RHE, and a limiting current density (J_{lim}) of 6.05 mA cm⁻² (Figure 3a and 3b). JUC-651 demonstrated higher catalytic activity than TFPPy-PyTTA-COF, with corresponding E_{onset} , $E_{1/2}$, and J_{lim} values of 0.854 V *vs* RHE, 0.68 V *vs* RHE, and 5.63 mA cm⁻², respectively. In contrast, TFPPy-PyTTA-COF displayed lower E_{onset} (0.795 V *vs* RHE), $E_{1/2}$ (0.62 V *vs* RHE), and a smaller J_{lim} (5.14 mA cm⁻²) (Figure 3a and 3b). The redox kinetic behavior of DBP-COFs was investigated using the Tafel slopes method, revealing Tafel slopes of 66.2 mV dec⁻¹ for JUC-650 and 69.5 mV dec⁻¹ for JUC-651, respectively, while TFPPy-PyTTA-COF exhibited a larger Tafel slope of 71.6 mV dec⁻¹ (Table S1 and Figure S25). These results indicated that JUC-650 exhibited faster ORR kinetic behavior compared to the other samples. Furthermore, LSV curves were obtained at different rotation rates (400-2500 rpm, Figures S29-S33), and the electron transfer numbers (n) of JUC-650, JUC-651, and TFPPy-PyTTA-COF were determined from Koutecky-Levich (K-L) plots at 0.2-0.5 V *vs* RHE to be 3.86, 3.54, and 3.15, respectively (Figure 3b, Table S1 and Figures S34-S37).

Electrochemical double-layer capacitance (C_{dl}) measurements were performed to elucidate the electrochemically active surface areas (ECSA) of the catalysts (Figures

S38-S42). As shown in Figure 3c, the C_{dl} value of JUC-650 (9.3 mF cm^{-2}) was larger than that of JUC-651 (7.7 mF cm^{-2}) and TFPPy-PyTTA-COF (2.9 mF cm^{-2}). Sequentially, the turnover frequency (TOF) at 0.7 V vs RHE and the mass activity of the COFs were determined to assess their intrinsic activity. JUC-650 exhibited a higher TOF value of 0.0026 s^{-1} compared to JUC-651 (0.0021 s^{-1}), and its mass activity (2.68 A g^{-1}) was also higher than that of JUC-651 (2.35 A g^{-1} , Figure 3d). These results indicate that JUC-650 exhibits more efficient utilization of active sites, which may be attributed to the modulation of structural electronic properties by the combination of ligands with different degrees of conjugation. Later on, the electrochemical impedance spectra (EIS) of DBP-COFs were determined in 0.1 M KOH aqueous solution. As a result, the charge transfer resistances of JUC-650 and JUC-651 were determined to be $284 \text{ } \Omega$ and $340 \text{ } \Omega$, respectively, indicating that JUC-650 possesses more efficient electron transfer capability (Figures S34). In addition, the durability of the synthetic COFs was evaluated at 0.7 V vs RHE for 25 h, revealing only 6.53% current density loss for JUC-650, indicating its good stability in alkaline solutions (Figure 3e). Then, negligible current density loss was observed in the presence of methanol for 200 s at 0.7 V , indicating the excellent tolerance of DBP-COFs to small organic molecules (Figure 3f). Lastly, post-testing characterization of the DBP-COFs revealed the preservation of their original framework structure (Figures S46-S48). In addition, compared with the reported performance of metal-free COF-based ORR electrocatalysts, JUC-650 is one of the best ORR catalysts to date (Figure 3g and Table 1). Figure 4 depicts the ORR

catalytic mechanism of JUC-650, which approaches a four-electron ($4e^-$) transfer mechanism.

2.4 Zn-air battery performance

Based on the excellent ORR performance of DBP-COFs, an aqueous Zn-air battery (ZAB) was assembled using JUC-650 as an electrocatalyst for the air cathode to evaluate its potential application. The power density curve was closely related to the discharge polarization curve, and the discharge polarization curve of JUC-650-based ZAB decreased steadily below 0.6 V. The peak power density of JUC-650-based ZAB reached 101.5 mW cm^{-2} at 0.35 V (Figure 5a). As shown in Figure 5b, the open circuit voltage (OCV) of the JUC-650-based ZAB stabilized at 1.38 V, close to that of commercial Pt/C. Subsequently, a "COF" LED screen was successfully powered up using the JUC-650-based ZAB, demonstrating its feasibility in practical applications. The JUC-650-based ZAB also exhibited potential stability values of 1.01, 0.85, and 0.68 V at different discharge current densities of 25, 50, and 100 mA cm^{-2} , respectively (Figure 5c). Besides, the specific capacity of JUC-650-based ZAB was calculated by normalizing the mass of consumed Zn, resulting in a high specific capacity of $722.6 \text{ mAh g}_{\text{Zn}}^{-1}$ at 50 mA cm^{-2} , which is also comparable to that of commercial Pt/C (Figure 5d). In summary, DBP-COFs exhibited great potential for application in energy devices.

2.5 DFT Calculations

DFT calculations were performed to elucidate the distinct ORR activity of carbon atoms in the samples (Figure 6 and Figures S51-57). The optimizations for all

calculations were carried out using the spin-unrestricted DFT method implemented in the DMol3 code. Electrostatic potential surface (ESP) maps of these COFs confirmed that combining different building units could adjust the charge distribution. As shown in Figure 6a, nitrogen-doped JUC-650 exhibited prominent electron-rich regions and well-defined π conjugation, which can enhance the electrophilicity of Lewis basic carbon atoms as active sites. This phenomenon facilitates the adsorption of oxygen, thereby accelerating the rate-determining step (RDS) of the ORR process.^[7,8] We further investigated the ORR Gibbs free energy (ΔG) of potential active sites in the three COFs. The results revealed that the RDS of our samples was the formation of OOH* from O₂ during the ORR process. The RDS energy barrier of the C=N(C) groups in JUC-650 (1.09 eV) and JUC-651 (1.20 eV) was much lower than that of TFPPy-PyTTA-COF (1.87 eV, Figure 6b and Figure S51), indicating that JUC-650 exhibited the highest adsorption energy for OOH* and promoted the forward direction of the ORR reaction. These findings also confirm that C=N(C) serves as the active center for the ORR process in these three COFs, and provide additional evidence that the combination of ligands with different degrees of conjugation can modulate the ORR activity. Moreover, the density of states (DOS) also showed that DBP-COFs had excellent electrical conductivity (Figure 6c).

3. Conclusion

In conclusion, we have successfully synthesized two metal-free DBP-COFs (JUC-650 and JUC-651) by employing dibenzo[a,c]phenazine as the central building unit in our innovative design. These newly synthesized COFs exhibit unique 2D pore structures,

high crystallinity, and a high specific surface area, while demonstrating excellent catalytic performance for the oxygen ORR. Among them, JUC-650 stands out as one of the most promising metal-free COF-based ORR catalysts, with a high onset potential of 0.90 V vs RHE and a half-wave potential of 0.72 V vs RHE. Furthermore, JUC-650 shows remarkable catalytic stability and methanol tolerance, with only a 6.53% current density loss observed in long-term stability tests. When utilized as an air cathode catalyst in a water-based ZAB, JUC-650-based ZAB exhibits a stable open circuit voltage of 1.38 V and an ultra-high specific capacity of 722.6 mAh g_{Zn}⁻¹, approaching the performance level of commercial Pt/C. These results highlight the vast potential of DBP-COFs in novel energy storage and conversion devices. Additionally, DFT calculations indicate that the Schiff-base carbon atoms, with enhanced electrophilic properties, serve as the active sites for ORR, emphasizing the precise control of electronic configuration by adjusting the frameworks. The strategy of tuning catalytic activity through the selection of different building units offers further guidance and possibilities for developing efficient metal-free carbon-based electrocatalysts and achieving precise modulation of active sites in the future.

Supporting Information

Supporting Information is available from the Wiley Online Library or from the author.

Acknowledgements

This work was supported by National Key R&D Program of China (2022YFB3704900 and 2021YFF0500500), National Natural Science Foundation of

China (22025504, 21621001, and 22105082), the SINOPEC Research Institute of Petroleum Processing, "111" project (BP0719036 and B17020), the Taishan Scholars Program (No. tsqn202211124), China Postdoctoral Science Foundation (2020TQ0118 and 2020M681034), and the program for JLU Science and Technology Innovative Research Team.

Conflict of Interest

The authors declare no conflict of interest.

Reference

- [1] L. Dai, Y. Xue, L. Qu, H. J. Choi, J. B. Baek, *Chem. Rev.* **2015**, *115*, 4823.
- [2] X. Liu, L. Dai, *Nat. Rev. Mater.* **2016**, *1*, 16064.
- [3] S. L. Zhao, D. W. Wang, R. Amal, L. M. Dai, *Adv. Mater.* **2019**, *31*, 22.
- [4] L. J. Yang, J. L. Shui, L. Du, Y. Y. Shao, J. Liu, L. M. Dai, Z. Hu, *Adv. Mater.* **2019**, *31*, 20.
- [5] R. G. Ma, G. X. Lin, Y. Zhou, Q. Liu, T. Zhang, G. C. Shan, M. H. Yang, J. C. Wang, *Npj Comput. Mater.* **2019**, *5*, 78.
- [6] S. K. Singh, K. Takeyasu, J. Nakamura, *Adv. Mater.* **2019**, *31*, 17.
- [7] K. Gong, F. Du, Z. Xia, M. Durstock, L. Dai, *Science.* **2009**, *323*, 760.
- [8] D. Guo, R. Shibuya, C. Akiba, S. Saji, T. Kondo, J. Nakamura, *Science.* **2016**, *351*, 361.
- [9] Z. J. Zhao, B. B. Wang, Z. H. You, Q. K. Zhang, W. C. Song, X. J. Long, *Small.* **2023**, *19*, 9.
- [10] C. Tang, Q. Zhang, *Adv. Mater.* **2017**, *29*, 1604103.

- [11] K. Srinivas, D. W. Liu, F. Ma, A. R. Chen, Z. H. Zhang, Y. Wu, Q. Wu, Y. F. Chen, *Small*. **2023**, 11.
- [12] Y. Shu, Y. Takada, R. Takada, Y. Taniguchi, K. Miyake, Y. Uchida, C. Y. Kong, N. Nishiyama, *Adv. Mater. Interfaces*. **2023**, 10, 2300088.
- [13] Q. Yang, Z. C. Xiao, D. B. Kong, T. L. Zhang, X. G. Duan, S. K. Zhou, Y. Niu, Y. D. Shen, H. Q. Sun, S. B. Wang, L. J. Zhi, *Nano Energy*. **2019**, 66, 8.
- [14] H. B. Yang, J. W. Miao, S. F. Hung, J. Z. Chen, H. B. Tao, X. Z. Wang, L. P. Zhang, R. Chen, J. J. Gao, H. M. Chen, L. M. Dai, B. Liu, *Sci. Adv.* **2016**, 2, 11.
- [15] Q. R. Zhang, Y. G. Chen, J. Pan, R. Daiyan, E. C. Lovell, J. M. Y. Yun, R. Amal, X. Y. Lu, *Small*. **2023**, 30.
- [16] Y. J. Han, Y. Q. Shen, Y. H. Song, H. X. Zhang, P. Z. Liu, J. J. Guo, *ChemElectroChem*. **2022**, 9, 8.
- [17] G. Y. Ye, S. Q. Liu, K. M. Zhao, Z. He, *Angew. Chem. Int. Edit.* **2023**, 62, 10.
- [18] R. L. Song, X. T. Cao, J. Xu, X. S. Zhou, X. Wang, N. Y. Yuan, J. N. Ding, *Nanoscale*. **2021**, 13, 6174.
- [19] H. M. Zhang, Y. Wang, D. Wang, Y. B. Li, X. L. Liu, P. R. Liu, H. G. Yang, T. C. An, Z. Y. Tang, H. J. Zhao, *Small*. **2014**, 10, 3371.
- [20] C. J. Lei, Q. Zheng, F. P. Cheng, Y. Hou, B. Yang, Z. J. Li, Z. H. Wen, L. C. Lei, G. L. Chai, X. L. Feng, *Adv. Funct. Mater.* **2020**, 30, 9.
- [21] C. Zhang, W. Q. Shen, K. Guo, M. Xiong, J. Zhang, X. Lu, *J. Am. Chem. Soc.* **2023**, 145, 11589.
- [22] D. Li, J. Yi, G. Chang, J. Chen, H. Liu, J. Wang, Y. Hu, Y. Xia, D. Yang, X. Yao,

- Chem.* **2018**, *4*, 2345.
- [23] H. Zhang, M. Zhu, O. G. Schmidt, S. Chen, K. Zhang, *Adv. Energy Sustain. Res.* **2021**, *2*, 2000090.
- [24] C. Ouyang, X. Wang, *Inorg. Chem. Front.* **2020**, *7*, 28.
- [25] Y. P. Zhu, C. X. Guo, Y. Zheng, S. Z. Qiao, *Accounts Chem. Res.* **2017**, *50*, 915.
- [26] H. Chen, X. Liang, Y. P. Liu, X. Ai, T. Asefa, X. X. Zou, *Adv. Mater.* **2020**, *32*, 32.
- [27] X. Long, D. Li, B. Wang, Z. Jiang, W. Xu, B. Wang, D. Yang, Y. Xia, *Angew. Chem. Int. Ed.* **2019**, *58*, 11369.
- [28] A. P. Cote, A. I. Benin, N. W. Ockwig, M. O'Keeffe, A. J. Matzger, O. M. Yaghi, *Science.* **2005**, *310*, 1166.
- [29] F. Jin, E. Lin, T. Wang, S. Geng, T. Wang, W. Liu, F. Xiong, Z. Wang, Y. Chen, P. Cheng, *J. Am. Chem. Soc.* **2022**, *144*, 5643.
- [30] C. Yu, H. Li, Y. Wang, J. Suo, X. Guan, R. Wang, V. Valtchev, Y. Yan, S. Qiu, Q. Fang, *Angew. Chem. Int. Ed.* **2022**, *61*, e202117101.
- [31] Y. Y. Zhang, H. Li, J. H. Chang, X. Y. Guan, L. X. Tang, Q. R. Fang, V. Valtchev, Y. S. Yan, S. L. Qiu, *Small.* **2021**, *17*, 9.
- [32] F. Li, J. L. Kan, B. J. Yao, Y. B. Dong, *Angew. Chem. Int. Ed.* **2022**, *61*, e202115044.
- [33] Y. Z. Liu, J. X. Ren, Y. J. Wang, X. Zhu, X. Y. Guan, Z. S. Wang, Y. D. Zhou, L. K. Zhu, S. L. Qiu, S. X. Xiao, Q. R. Fang, *CCS Chem.* **2022**, *5*, 1.
- [34] W. J. Zhao, C. Y. Yu, J. Zhao, F. Q. Chen, X. Y. Guan, H. Li, B. Tang, G. T. Yu, V.

- Valtchev, Y. S. Yan, S. L. Qiu, Q. R. Fang, *Small*. **2021**, *17*, 9.
- [35] E. Hamzehpoor, C. Ruchlin, Y. Z. Tao, C. H. Liu, H. M. Titi, D. F. Perepichka, *Nat. Chem.* **2023**, *15*, 83.
- [36] X. Y. Wang, B. B. Shi, H. Yang, J. Y. Guan, X. Liang, C. Y. Fan, X. D. You, Y. A. Wang, Z. Zhang, H. Wu, T. Cheng, R. N. Zhang, Z. Y. Jiang, *Nat. Commun.* **2022**, *13*, 9.
- [37] R. Wang, Y. S. Zhou, Y. Zhang, J. Xue, J. Caro, H. H. Wang, *Adv. Mater.* **2022**, *34*, 10.
- [38] W. K. Wang, W. W. Zhao, T. T. Chen, Y. Bai, H. T. Xu, M. Y. Jiang, S. J. Liu, W. Huang, Q. Zhao, *Adv. Funct. Mater.* **2021**, *31*, 9.
- [39] S. Cao, B. Li, R. M. Zhu, H. Pang, *Chem. Eng. J.* **2019**, *355*, 602.
- [40] H. Wang, H. Wang, Z. W. Wang, L. Tang, G. M. Zeng, P. Xu, M. Chen, T. Xiong, C. Y. Zhou, X. Y. Li, D. N. Huang, Y. Zhu, Z. X. Wang, J. W. Tang, *Chem. Soc. Rev.* **2020**, *49*, 4135.
- [41] P. F. Wei, M. Z. Qi, Z. P. Wang, S. Y. Ding, W. Yu, Q. Liu, L. K. Wang, H. Z. Wang, W. K. An, W. Wang, *J. Am. Chem. Soc.* **2018**, *140*, 4623.
- [42] Y. F. Zhi, Z. R. Wang, H. L. Zhang, Q. C. Zhang, *Small*. **2020**, *16*, 21.
- [43] Y. Yusran, Q. Fang, V. Valtchev, *Adv. Mater.* **2020**, *32*, 2002038.
- [44] J. M. Rotter, R. Guntermann, M. Auth, A. Mahringer, A. Sperlich, V. Dyakonov, D. D. Medina, T. Bein, *Chem.Sci.* **2020**, *11*, 12843.
- [45] Q. Wu, M. J. Mao, Q. J. Wu, J. Liang, Y. B. Huang, R. Cao, *Small*. **2021**, *17*, 2004933.

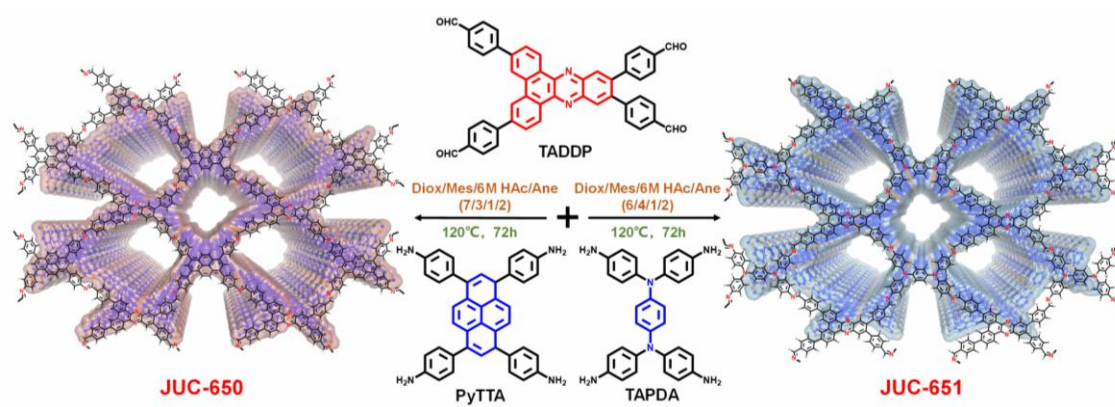
- [46] X. Ren, C. Li, W. Kang, H. Li, N. Ta, S. Ye, L. Hu, X. Wang, C. Li, Q. Yang, *CCS Chem.* **2022**, *4*, 2429.
- [47] X. J. Zhao, P. Pachfule, S. Li, T. Langenhahn, M. Y. Ye, C. Schlesiger, S. Praetz, J. Schmidt, A. Thomas, *J. Am. Chem. Soc.* **2019**, *141*, 6623.
- [48] H. Furukawa, O. M. Yaghi, *J. Am. Chem. Soc.* **2009**, *131*, 8875.
- [49] H. Chen, W. L. Liu, A. Laemont, C. Krishnaraj, X. Feng, F. Rohman, M. Meledina, Q. Q. Zhang, R. Van Deun, K. Leus, P. van der Voort, *Angew. Chem. Int. Edit.* **2021**, *60*, 10820.
- [50] L. H. Li, Y. H. Ma, H. H. Yang, N. Wu, L. P. Peng, J. J. Wang, *ACS Appl. Polym. Mater.* **2023**, *5*, 784.
- [51] Z. F. Zhao, D. Zheng, M. L. Guo, J. Y. Yu, S. N. Zhang, Z. J. Zhang, Y. Chen, *Angew. Chem. Int. Edit.* **2022**, *61*, 8.
- [52] C. Y. Lin, L. Zhang, Z. Zhao, Z. Xia, *Adv. Mater.* **2017**, *29*, 1606635.
- [53] J. Zhang, J. Zhang, F. He, Y. Chen, J. Zhu, D. Wang, S. Mu, H. Y. Yang, *Nano-Micro Lett.* **2021**, *13*, 65.
- [54] S. Mondal, B. Mohanty, M. Nurhuda, S. Dalapati, R. Jana, M. Addicoat, A. Datta, B. K. Jena, A. Bhaumik, *ACS Catalysis.* **2020**, *10*, 5623.
- [55] D. Li, C. Li, L. Zhang, H. Li, L. Zhu, D. Yang, Q. Fang, S. Qiu, X. Yao, *J. Am. Chem. Soc.* **2020**, *142*, 8104.
- [56] S. Chang, C. Li, H. Li, L. Zhu, Q. Fang, *Chem Res Chinese U.* **2022**, *38*, 396.
- [57] C. Liu, F. Liu, H. Li, J. Chen, J. Fei, Z. Yu, Z. Yuan, C. Wang, H. Zheng, Z. Liu, *ACS nano.* **2021**, *15*, 3309.

- [58] X. Yu, Y. Ma, C. Li, X. Guan, Q. Fang, S. Qiu, *Chem Res Chinese U.* **2022**, *38*, 167.
- [59] J. Jia, J. Li, S. Ma, Z. Zhang, X. Liu, *Macromol. Rapid. Comm.* **2022**, *44*, 2200717.
- [60] Q. Yan, H. Xu, X. Jing, H. Hu, S. Wang, C. Zeng, Y. Gao, *RSC Adv.* **2020**, *10*, 17396.
- [61] Materials Studio ver. 7.0, S. Diego, *Accelrys Inc*, **2013**.
- [62] J.-Y. Yue, Y.-T. Wang, X. Wu, P. Yang, Y. Ma, X.-H. Liu, B. Tang, *ChemComm.* **2021**, *57*, 12619.
- [63] S. Roy, S. Mari, M. K. Sai, S. C. Sarma, S. Sarkar, S. C. Peter, *Nanoscale.* **2020**, *12*, 22718.
- [64] J. H. Park, C. H. Lee, J. M. Ju, J. H. Lee, J. Seol, S. U. Lee, J. H. Kim, *Adv. Funct. Mater.* **2021**, *31*, 2101727.
- [65] S. Wu, M. Li, H. Phan, D. Wang, T. S. Herng, J. Ding, Z. Lu, J. Wu, *Angew. Chem. Int. Ed.* **2018**, *57*, 8007.
- [66] M. Martínez-Fernández, E. Martínez-Periñán, S. Royuela, J. I. Martínez, F. Zamora, E. Lorenzo, J. L. Segura, *Appl. Mater. Today.* **2022**, *26*, 101384.
- [67] P. García-Arroyo, E. Martínez-Periñán, J. J. Cabrera-Trujillo, E. Salagre, E. G. Michel, J. I. Martínez, E. Lorenzo, J. L. Segura, *Nano Res.* **2022**, *15*, 3907.
- [68] Z. You, B. Wang, Z. Zhao, Q. Zhang, W. Song, C. Zhang, X. Long, Y. Xia, *Adv. Mater.* **2023**, *35*, 2209129.
- [69] X. Yan, B. Wang, J. Ren, X. Long, D. Yang, *Angew. Chem. Int. Ed.* **2022**, *134*,

e202209583.

- [70] S. Royuela, E. Martínez-Periñán, M. P. Arrieta, J. I. Martínez, M. M. Ramos, F. Zamora, E. Lorenzo, J. L. Segura, *ChemComm.* **2020**, *56*, 1267.
- [71] J. Liu, Y. Hu, J. Cao, *Catal. Commun.* **2015**, *66*, 91.
- [72] J. Chang, C. Li, X. Wang, D. Li, J. Zhang, X. Yu, H. Li, X. Yao, V. Valtchev, S. Qiu, Q. Fang, *Nano-Micro Lett.* **2023**, *15*, 159.

Figures and captions:



Scheme 1. Synthesis strategy of DBP-COFs (JUC-650 and JUC-651).

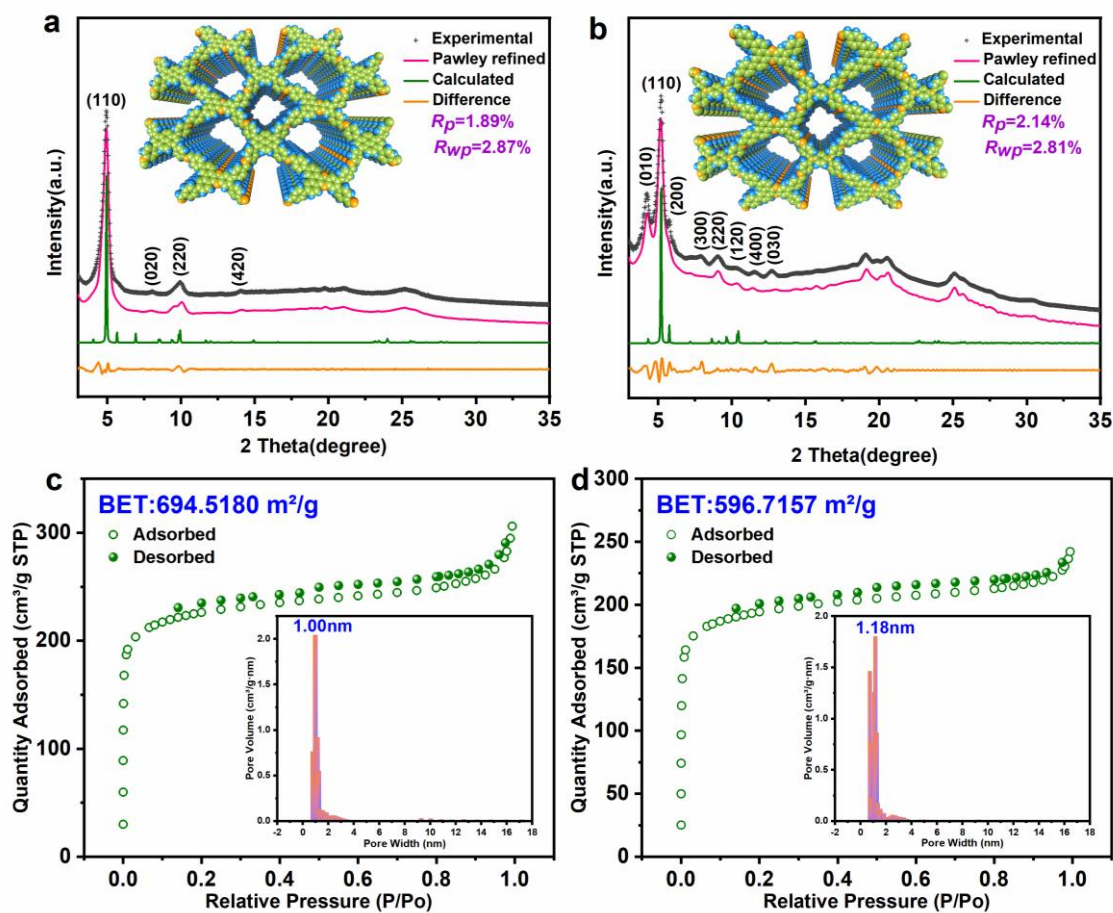


Figure 1. Powder XRD patterns and crystal structural (inset) of JUC-650 (a) and JUC-651 (b). N₂ adsorption-desorption isotherms and pore size distribution (inset) for JUC-570 (c) and JUC-571 (d) at 77 K.

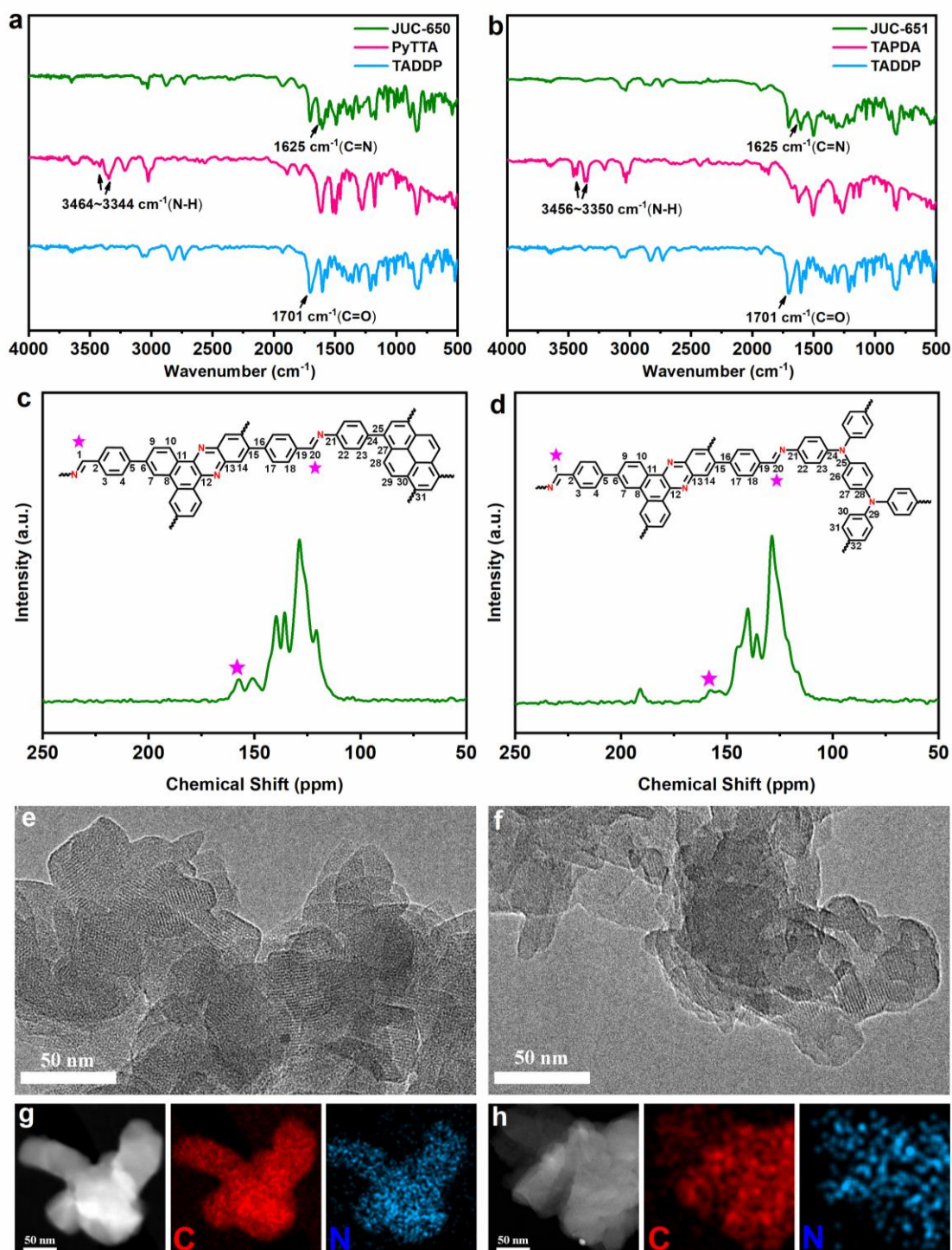


Figure 2. FT-IR spectra of JUC-650 (a) and JUC-651 (b). Solid-state ¹³C CP/MAS-NMR spectra of JUC-650 (c) and JUC-651 (d). TEM image of JUC-650 (e) and JUC-651 (f). TEM image and the related elemental mapping images of carbon, and nitrogen for JUC-650 (g) and JUC-651 (h).

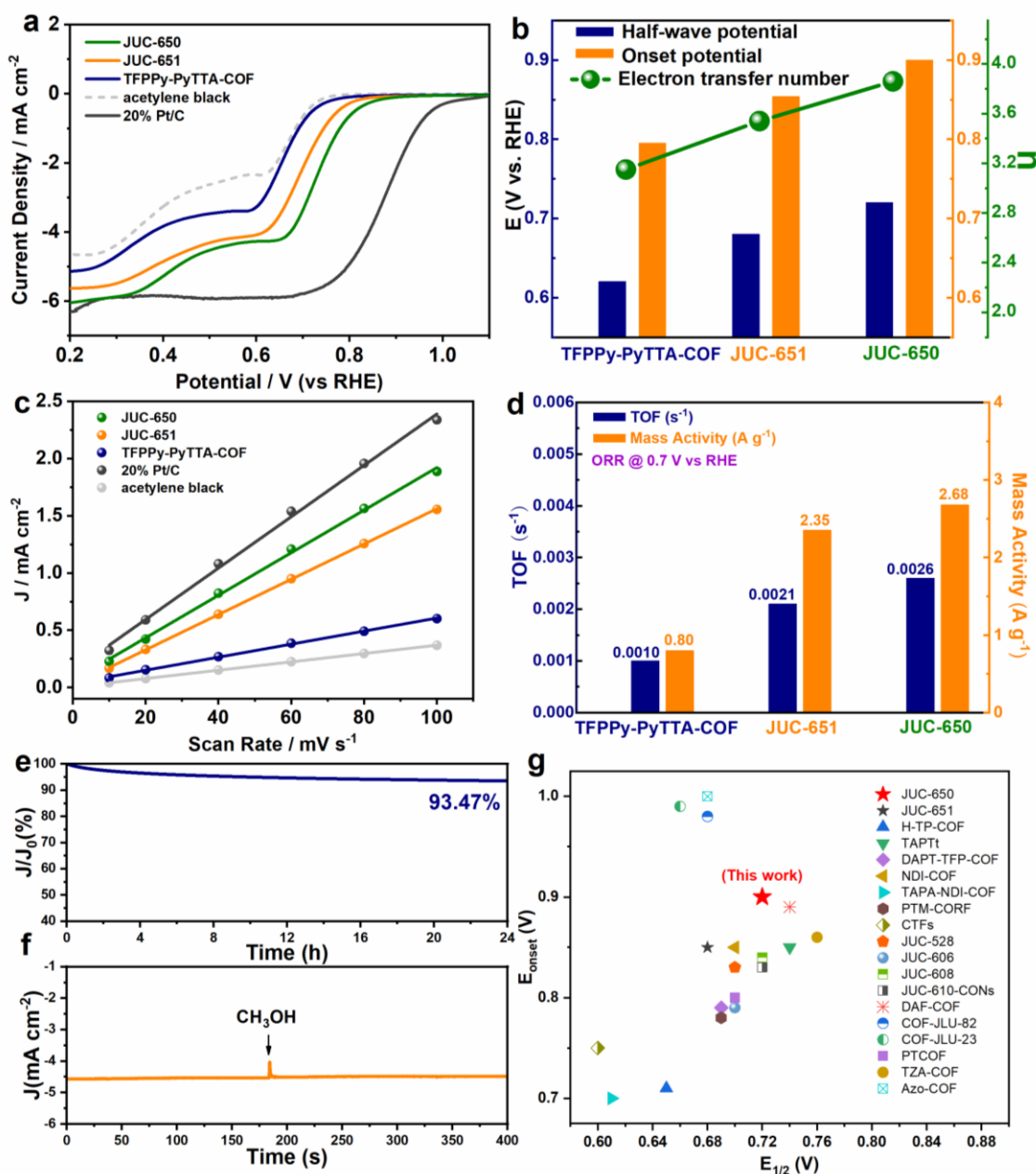


Figure 3. a) LSV curves of JUC-650, JUC-651, TFPPy-PyTTA-COF, 20% Pt/C, and acetylene black at 1600 rpm in O₂-saturated 0.1 M KOH electrolyte; b) Comparison of half-wave potential, onset potential, electron transfer number; c) Estimated electrochemical double-layer capacitance (C_{dl}); d) Comparison of TOF and mass activity; e) Long-term stability test of JUC-650 at 0.7 V (vs RHE); f) poisoning

resistance test of JUC-650 at 0.7 V (*vs* RHE); g) Comparison of onset and half-wave potentials of metal-free COFs as ORR electrocatalysts.

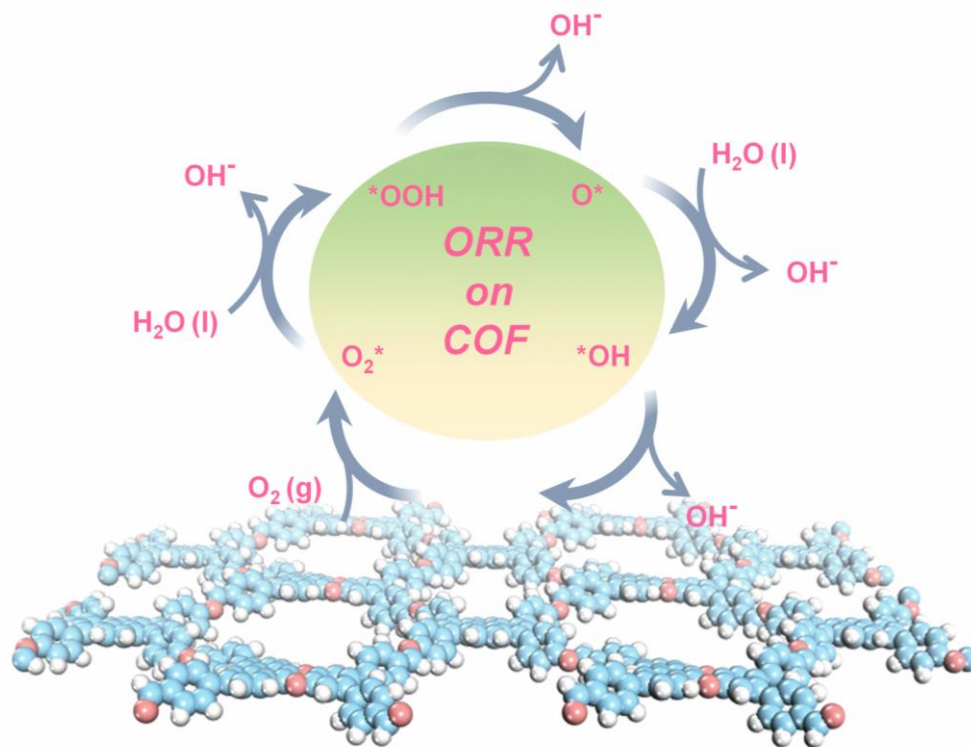


Figure 4. Proposed ORR processes on JUC-650.

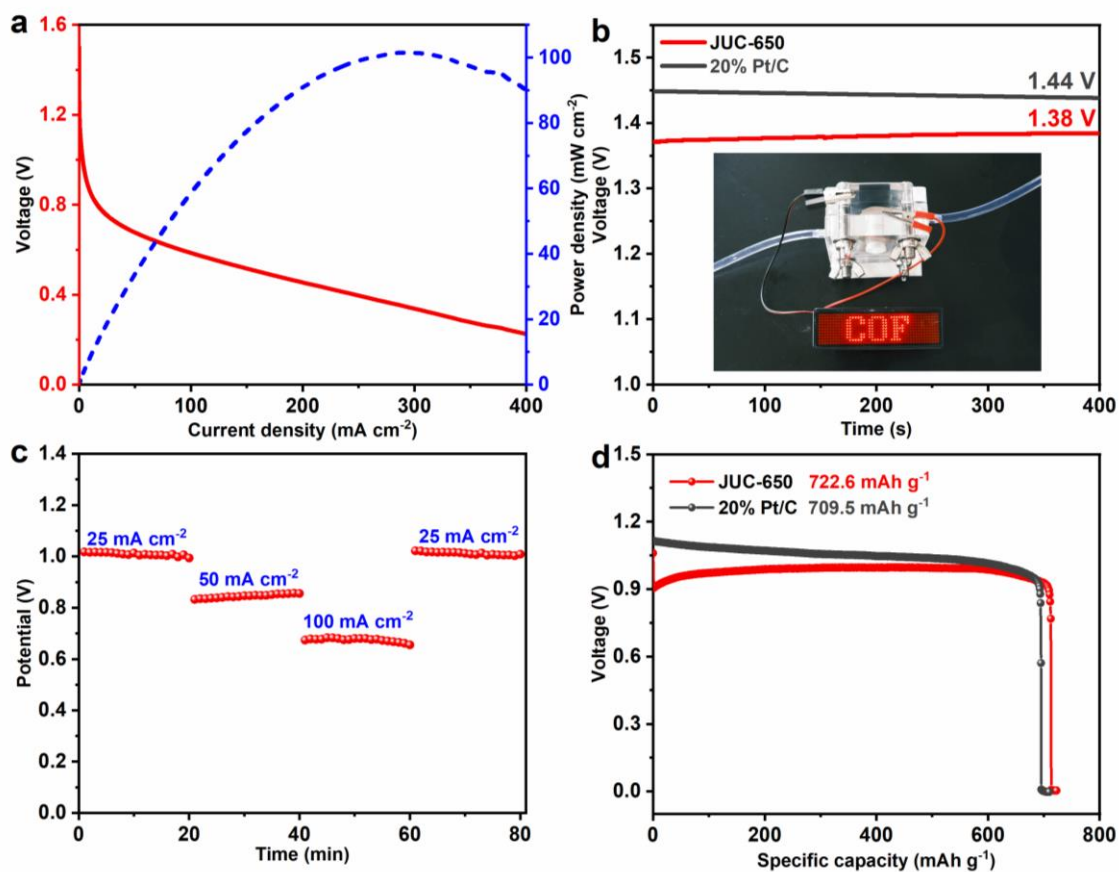


Figure 5. a) Power density curves of JUC-650-based ZAB; b) Open circuit voltage of JUC-650-based ZAB and 20% Pt/C as well as the photograph of a “COF” LED screen powered by JUC-650-based ZAB; c) Discharge curves of JUC-650-based ZAB at different current densities (25, 50, 100, and 25 mA cm⁻²); d) Specific capacities of the JUC-650-based ZAB and 20% Pt/C.

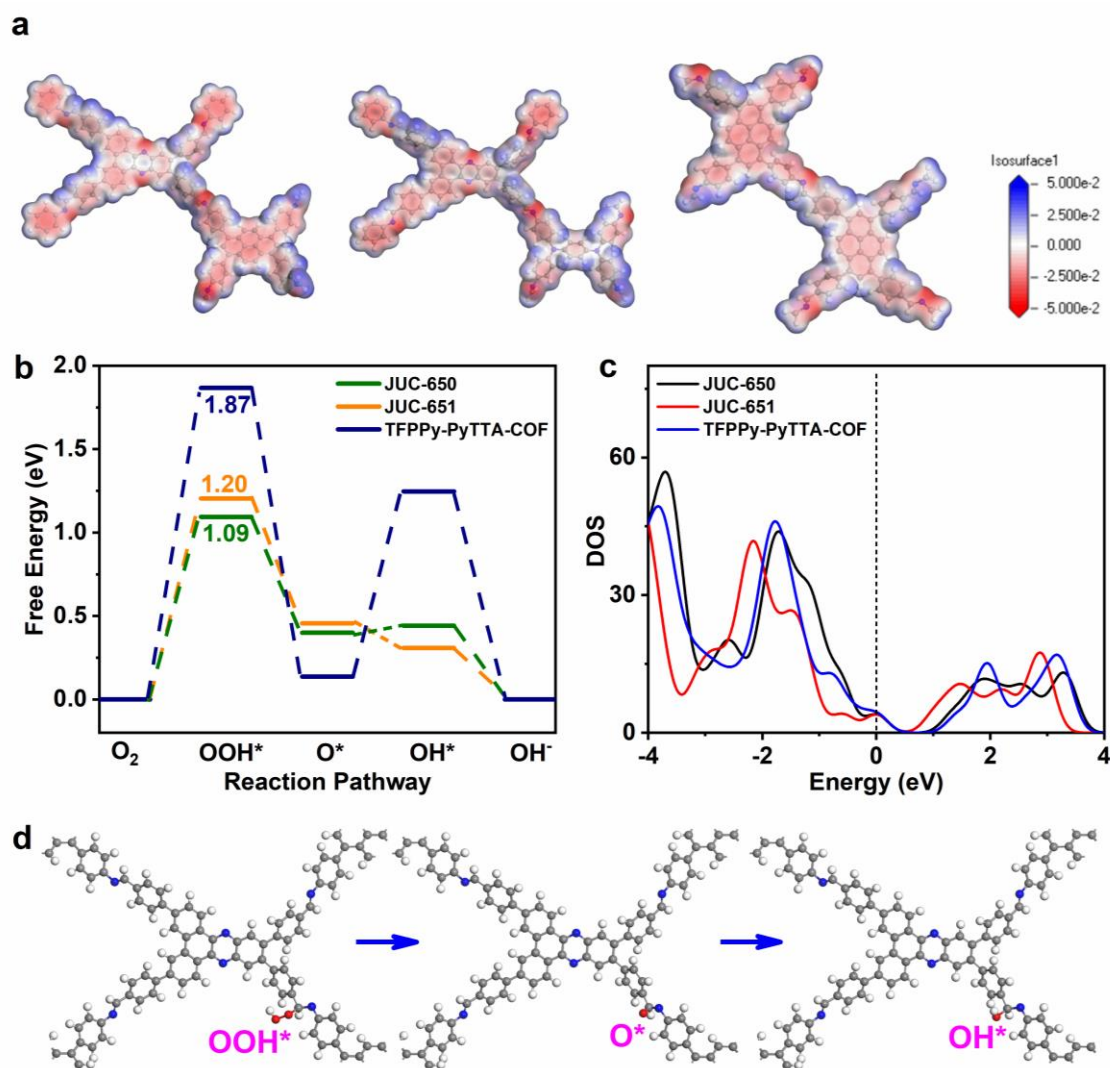


Figure 6. a) The ESP maps of JUC-650, JUC-651, and TFPPy-PyTTA-COF calculated by DFT; b) Free energy diagrams of C=N(C) for JUC-650, JUC-651, and TFPPy-PyTTA-COF; c) DOS for JUC-650, JUC-651, and TFPPy-PyTTA-COF; d) Diagram of the three steps of ORR reaction on the surface of JUC-650 after structural optimization.

Table 1. Comparative ORR activity table with recently reported metal-free COF electrocatalysts.

Materials	Half-wave Potential / V	Onset Potential/V	Tafel slope / mV dec ⁻¹	electron transfer number (n)	Ref.
JUC-650	0.72	0.90	66.2	3.86	This work
JUC-651	0.68	0.85	69.5	3.54	This work
JUC-528	0.7	0.83	65.9	3.81	2020 ^[55]
JUC-608	0.72	0.84	85	4.285	2022 ^[56]
TAPTt	0.74	0.85	/	3.42	2021 ^[57]
JUC-606	0.70	0.79	59.88	3.2	2022 ^[58]
COF-JLU-82	0.68	0.98	72.79	4.64	2022 ^[59]
COF-JLU-23	0.66	0.99	81.96	3.65	2022 ^[59]
H-TP-COF	0.65	0.71	104	/	2021 ^[62]
TZA-COF	0.76	0.86	67.05	2.5-2.9	2020 ^[63]
PTCOF	0.7	0.8	124	/	2021 ^[64]
PTM-CORF	0.69	0.78	/	3.89	2018 ^[65]
TAPA-NDI-COF	0.61	0.70	84.2	3.3-3.5	2022 ^[66]
DAPT-TFP-COF	0.69	0.79	33.1	3.6	2022 ^[67]
DAF-COF	0.74	0.89	65.1	3.88	2023 ^[68]
Azo-COF	0.68	0.88	89	3.10-3.30	2022 ^[69]
NDI-COF	0.70	0.85	/	3.6	2022 ^[70]
CTFs	0.6	0.75	/	3.6	2015 ^[71]
JUC-610-CONs	0.72	0.83	61.95	3.82	2023 ^[72]

TOC:

Two metal-free dibenzo[a,c]phenazine-based COFs (DBP-COFs) were synthesized and employed as ORR electrocatalysts. Among them, JUC-650 exhibited excellent catalytic performance for ORR in alkaline electrolyte, with an onset potential of 0.90 V *vs* RHE and a half-wave potential of 0.72 V *vs* RHE, which has been confirmed as one of the best metal-free COF-based ORR electrocatalysts so far.

Keywords: covalent organic framework, oxygen reduction reaction, metal-free electrocatalyst, porous materials, Zn-air battery

Jianchuan Liu, Jie Zhao, Cuiyan Li, Yaozu Liu, Daohao Li, Hui Li, Valentin Valtchev, Shilun Qiu, Yujie Wang* and Qianrong Fang**

Precise Modulation of Carbon Activity Sites in Metal-Free Covalent Organic Frameworks for Enhanced Oxygen Reduction Electrocatalysis

